Zhao, L., Zheng, X., Jiao, J., Han, F., Zhou, B., Fan, P., Jia, L., and Ma, Y., 2023, Geochronology, petrogenesis, and magmatic oxidation state of the Mangling intrusive complex, Northern Qinling Belt, Central China: Implications for magma fertility and tectonic setting: GSA Bulletin, https://doi.org/10.1130/B36714.1.

Supplemental Material

Supplemental Text. Analytical Methods.

Figure S1. Cathodoluminescence images of representative zircons for U-Pb dating and Lu-Hf isotope analyses for the Mangling intrusive complex.

Figure S2. Chondrite-normalized rare earth element patterns of analyzed zircons for the Mangling intrusive complex.

Figure S3. Field photographs showing relationships of the granitic rocks of the Mangling intrusive complex.

Figure S4. Harker diagrams of selected major and trace elements against SiO_2 for the Mangling intrusive complex.

Table S1. Zircon U-Pb dating results for the doritic and granitic rocks of the Mangling intrusive complex.

Table S2. Whole-rock major- (wt%), trace- (ppm), and rare earth (ppm) element compositions for the dioritic and granitic rocks of the Mangling intrusive complex.

Table S3. Zircon trace element compositions (ppm) for the dioritic and granitic rocks of the Mangling intrusive complex.

Table S4. Zircon Lu-Hf isotopic data for the dioritic and granitic rocks of the Mangling intrusive complex.

Table S5. Summary of geochronological data for the Mangling intrusive complex.

Table S6. Zircon trace element compositions (ppm) for the mineralized granitic rocks of porphyry molybdenum deposits in Central and NE China.

ANALYTICAL METHODS

Zircon U-Pb Dating

By using conventional heavy liquid and magnetic techniques, zircons were separated from five representative dioritic (biotite diorite and biotite diorite enclave) and granitic rock samples (medium- to fine-grained and fine-grained monzogranite and K-feldspar granite) collected from the Mangling intrusive complex and then handpicked under a binocular microscope. The selected zircon grains were mounted in epoxy resin and polished to expose the crystal centers to observe their internal structure under cathodoluminescence (CL) imaging that was carried out at the Testing Center, Tuoyan Analytical Technology Co. Ltd. (Guangzhou, China) using a TESCAN MIRA3 field-emission scanning electron microprobe (FE-SEM).

In-situ U-Pb dating of zircon grains were performed at the Nanjing FocuMS Technology Co. Ltd. (Nanjing, China), using an Agilent Technologies 7700x quadrupole inductively coupled plasma-mass spectrometry (ICP-MS) coupled with a Resonetics RESOlution LR (193 nm ArF excimer) laser ablation system. During analysis, the laser ablation system has a spot diameter of 33 μm with a background acquisition of approximately 20 s followed by 40 s of data acquisition. 91500 zircon was used as external standard to correct instrumental mass discrimination and elemental fractionation during the ablation, whilst GJ-1 and Plešovice zircons were treated as quality control for geochronology. Trace elements of zircons were external calibrated against NIST SRM 610 with Si as internal standard. The detailed analytical technique is described by Li et al. (2011). Isotopic ratios of U-Pb dating were performed using ICPMSDataCal (Liu et al., 2008), and age calculation and plotting of concordia diagrams were performed using Isoplot/Ex 3.0 (Ludwig, 2003).

Whole-Rock Major and Trace Elements

Whole-rock major and trace element analyses were performed at the Key Laboratory of Western China's Mineral Resources and Geological Engineering, Ministry of Education and the State Key Laboratory of Isotope Geochemistry, Guangzhou Institute of Geochemistry, Chinese Academy of Sciences with sample names as "ML21-". Before analysis, following procedures should be performed for all the samples: (1) powder them to less than 200 meshes, (2) add Lithium Borate Flux (50%−50% $Li_2B_4O_7$−$LiBO_2$), and (3) mix them well and fuse in an auto fluxer between 1050 °C and 1100 °C. The X-ray fluorescence (XRF) spectrometry was used to analyze major elements with analytical precision better than 1%. For trace elements, HNO_3 + HF acid was used to digest whole-rock powder (50 mg) in steel-bomb coated Teflon beakers for two days in order to assure complete dissolution of the refractory minerals under high pressure. Then ICP-MS was used to analyze the solution, with analytical precision better than 5% for most trace elements.

Magmatic Oxidation State and Crystallization Temperature

Zircon Ce^{4+}/Ce^{3+} ratio and Ti-in-zircon thermometer were used to evaluate the magmatic oxidation state and crystallization temperatures of igneous rocks (Shen et al., 2015; Zhang et al., 2020), with detailed calculations in Ballard et al. (2002) and

Ferry and Watson (2007), respectively. Moreover, the zircon Eu anomalies (Eu/Eu*) were calculated based on normalized values of Sm and Gd concentrations by a conventional method, similar to the equation of whole-rock Eu anomalies. For the magmatic oxygen fugacity (fO_2), it is commonly estimated as relative fayalite-magnetite-quartz buffer (ΔFMQ) based on the incorporation of cerium into zircon, Ti-in-zircon temperature, and water content using the equation of Smythe and Brenan (2016). In this study, the Ti-in-zircon thermometer and zircon Ce^{4+}/Ce^{3+} and Eu/Eu* ratios were calculated to evaluate the magma nature of the Mangling intrusive complex using Geo-fO_2 software proposed by Li et al. (2019), with assumed SiO_2 and TiO_2 activity to be 1 and 0.7, respectively, because all samples from the Mangling intrusive complex of this study contain primary magmatic quartz and accessory mineral of sphene (Hao et al., 2021). For the water content, we use 4.0 wt% for the biotite diorite enclave (BDE), biotite diorite (BD), and medium- to fine-grained monzogranite (MMG) based on occurrence of hornblende in these samples (Hao et al., 2021) and 3.0 wt% for the fine-grained monzogranite (FMG) and K-feldspar granite (KG) because the hornblende begins to crystallize when the silicate melts contain more than 3.0 wt% H_2O (Burnham, 1979).

Zircon Lu-Hf Isotopes

Zircon Lu-Hf isotope analyses were performed at the Nanjing FocuMS Technology Co. Ltd. (Nanjing, China) using a Nu Plasma II multi-collector (MC)-ICP-MS (Wrexham, Wales, UK), coupled to a 193 nm excimer laser ablation system (RESOlution LR). Each acquisition incorporated 20 s background (gas blank), followed by spot diameter of 50 μm at 9 Hz repetition rate for 40 s. Using exponential correction for mass bias, the measured isotopic ratios of $^{176}Hf/^{177}Hf$ were normalized to $^{179}Hf/^{177}Hf$ = 0.7325. The measured $^{173}Yb/^{171}Yb$ and the natural ratio of 1.13268 (Chu et al., 2002) were used to calculate the mass bias factor of Yb. In IsotopeMaker, the natural ratios are $^{176}Yb/^{173}Yb$ = 0.79381 (Segal et al., 2003) and $^{176}Lu/^{175}Lu$ = 0.02656 (Wu et al., 2006). A more detailed analytical technique can be found in Zhang et al. (2015). The initial $^{176}Hf/^{177}Hf$ ratios were calculated according to the measured $^{176}Lu/^{177}Hf$ ratios and the ^{176}Lu decay constant of 1.867×10^{-11} year^{-1} (Söderlund et al., 2004), whereas $\varepsilon_{Hf}(t)$ values were calculated with chondritic values of $^{176}Hf/^{177}Hf$ = 0.0336 and $^{176}Lu/^{177}Hf$ = 0.282785 (Bouvier et al., 2008). The present-day $^{176}Hf/^{177}Hf$ = 0.28325 and $^{176}Lu/^{177}Hf$ = 0.0384 (Griffin et al., 2004) were used to define the depleted mantle line. Single-stage Hf model ages (T_{DM}) were calculated with $^{176}Lu/^{177}Hf$ = 0.0384 (Griffin et al., 2004) relative to the depleted mantle that is assumed to have linear isotopic growth ranging between $^{176}Hf/^{177}Hf$ = 0.279718 at 4.55 Ga and 0.283250 at present, whereas two-stage Hf model ages (T_{DM}^{C}) were calculated assuming a mean value of $^{176}Lu/^{177}Hf$ = 0.015 for the average continental crust (Griffin et al., 2002).

REFERENCES CITED

Ballard, J.R., Michael, P., and Campbell, H.I., 2002, Relative oxidation states of magmas inferred from Ce(IV)/Ce(III) in zircon: Application to porphyry copper deposits of northern Chile: Contributions to Mineralogy and Petrology, v. 144, p.

347–364, https://doi.org/10.1007/s00410-002-0402-5.

Bouvier, A., Vervoort, J.D., and Patchett, P.J., 2008, The Lu–Hf and Sm–Nd isotopic composition of CHUR: Constraints from unequilibrated chondrites and implications for the bulk composition of terrestrial planets: Earth and Planetary Science Letters, v. 273, p. 48–57, https://doi.org/10.1016/j.epsl.2008.06.010.

Burnham, C.W., 1979, Magmas and hydrothermal fluids, *in* Barnes, H.L., ed., Geochemistry of hydrothermal ore deposits: New York, JohnWiley, p. 71–136.

Chu, N.C., Taylor, R.N., Chavagnae, V., Nesbitt, R.W., Boela, R.M., Milton, J.A., German, C.R., Bayon, G., and Burton, K., 2002, Hf isotope ratio analysis using multi-collector inductively coupled plasma mass spectrometry: An evaluation of isobaric interference corrections: Journal of Analytical Atomic Spectrometry, v. 17, p. 1567–1574, https://doi.org/10.1039/b206707b.

Ferry, J.M., and Watson, E.B., 2007, New thermodynamic models and revised calibrations for the Ti-in-zircon and Zr-in-rutile thermometers: Contributions to Mineralogy and Petrology, v. 154, p. 429–437, https://doi.org/10.1007/s00410-007-0201-0.

Griffin, W.L., Belousova, E.A., Shee, S.R., Pearson, N.J., and O'Reily, S.Y., 2004, Archean crustal evolution in the northern Yilgarn Craton: U–Pb and Hf-isotope evidence from detrital zircons: Precambrian Research, v. 13l, p. 23l–282l, https://doi.org/10.1016/j.precamres.2003.12.011.

Griffin, W.L., Wang, X., Jackson, S.E., Pearson, N.J., O'Reilly, S.Y., Xu, X., and Zhou, X., 2002, Zircon chemistry and magma mixing SE China: In-situ analysis of Hf isotopes. Tonglu and Pingtan igneous complexes, Lithos, v. 61, p. 237–269, https://doi.org/10.1016/S0024-4937(02)00082-8.

Hao, H.D., Campbell, I.H., Cooke, D.R., Nakamura, E., and Sakaguchi, C., 2021, Geochronology, petrogenesis and oxidation state of the Northparkes igneous suite, New South Wales, Australia: Implications for magma fertility: Economic Geology, v. 116, p. 1161–1187, https://doi.org/10.5382/econgeo.4825.

Li, H., Zhang, H., Ling, M.X., Wang, F.Y., Ding, X., Zhou, J.B., Yang, X.Y., Tu, X.L., and Sun, W.D., 2011, Geochemical and zircon U–Pb study of the Huangmeijian A-type granite: Implications for geological evolution of the Lower Yangtze River belt: International Geology Review, v. 53, p. 499–525, https://doi.org/10.1080/00206814.2010.496202.

Li, W.K., Cheng, Y.Q., and Yang, Z.M., 2019. Geo-fO_2: Integrated software for analysis of magmatic oxygen fugacity: Geochemistry, Geophysics, Geosystems, v. 20, p. 2542–2555, https://doi.org/10.1029/2019GC008273.

Liu, Y.S., Hu, Z.C., Gao, S., Gunther, D., Xu, J., Gao, C.G., and Chen, H.H., 2008, In situ analysis of major and trace elements of anhydrous minerals by LA–ICP–MS without applying an internal standard: Chemical Geology, v. 257, p. 34–43, https://doi.org/10.1016/j.chemgeo.2008.08.004.

Ludwig, K.R., 2003, User's Manual for Isoplot 3.00. A Geochronological Toolkit for Microsoft Excel: Berkeley Geochronology Center Special Publication 4, 71 p.

Segal, I., Halicz, L., and Platzner, I.T., 2003, Accurate isotope ratio measurements of ytterbium by multiple collection inductively coupled plasma mass spectrometry applying erbium and hafnium in an improved double external normalization procedure: Journal of Analytical Atomic Spectrometry, v. 18, p. 1217–1223, https://doi.org/10.1039/b307016f.

Shen, P., Hattori, K., Pan, H.D., Jackson, S., and Seitmuratova, E., 2015, Oxidation condition and metal fertility of granitic magmas: Zircon trace-element data from porphyry Cu deposits in the Central Asian Orogenic Belt: Economic Geology, v. 110, p. 1861–1878, https://doi.org/10.2113/econgeo.110.7.1861.

Smythe, D.J., and Brenan, J.M., 2016, Magmatic oxygen fugacity estimated using zircon-melt partitioning of cerium: Earth and Planetary Science Letters, v. 453, p. 260–266, https://doi.org/10.1016/j.epsl.2016.08.013.

Söderlund, U., Patchett, P.J., Vervoort, J.D., and Isachsen, C.E., 2004, The ^{176}Lu decay constant determined by Lu–Hf and U–Pb isotope systematics of Precambrian mafic intrusions: Earth and Planetary Science Letters, v. 219, p. 311–324, https://doi.org/10.1016/S0012-821X(04)00012-3.

Wu, F.Y., Yang, Y.H., Xie, L.W., Yang, J.H., and Xu, P., 2006, Hf isotopic compositions of the standard zircons and baddeleyites used in U–Pb geochronology: Chemical Geology, v. 234, p. 105–126, https://doi.org/10.1016/j.chemgeo.2006.05.003.

Zhang, L., Ren, Z.Y., Xia, X.P., Li, J., and Zhang, Z.F., 2015, IsotopeMaker: A Matlab program for isotopic data reduction: International Journal of Mass Spectrometry, v. 392, p. 118–124, https://doi.org/10.1016/j.ijms.2015.09.019.

Zhang, Y., Tian, J., Hollings, P., Gong, L., Alburo, I., Berador, A.E., Francisco, D.G., Li, J., and Chen, H.Y., 2020, Mesozoic porphyry Cu–Au mineralization and associated adakite-like magmatism in the Philippines: Insights from the giant Atlas deposit: Mineralium Deposita, v. 55, p. 881–900, https://doi.org/10.1007/s00126-019-00907-2.

Figure S1. Cathodoluminescence images of representative zircons for U-Pb dating and Lu-Hf isotope analyses for the Mangling intrusive complex.

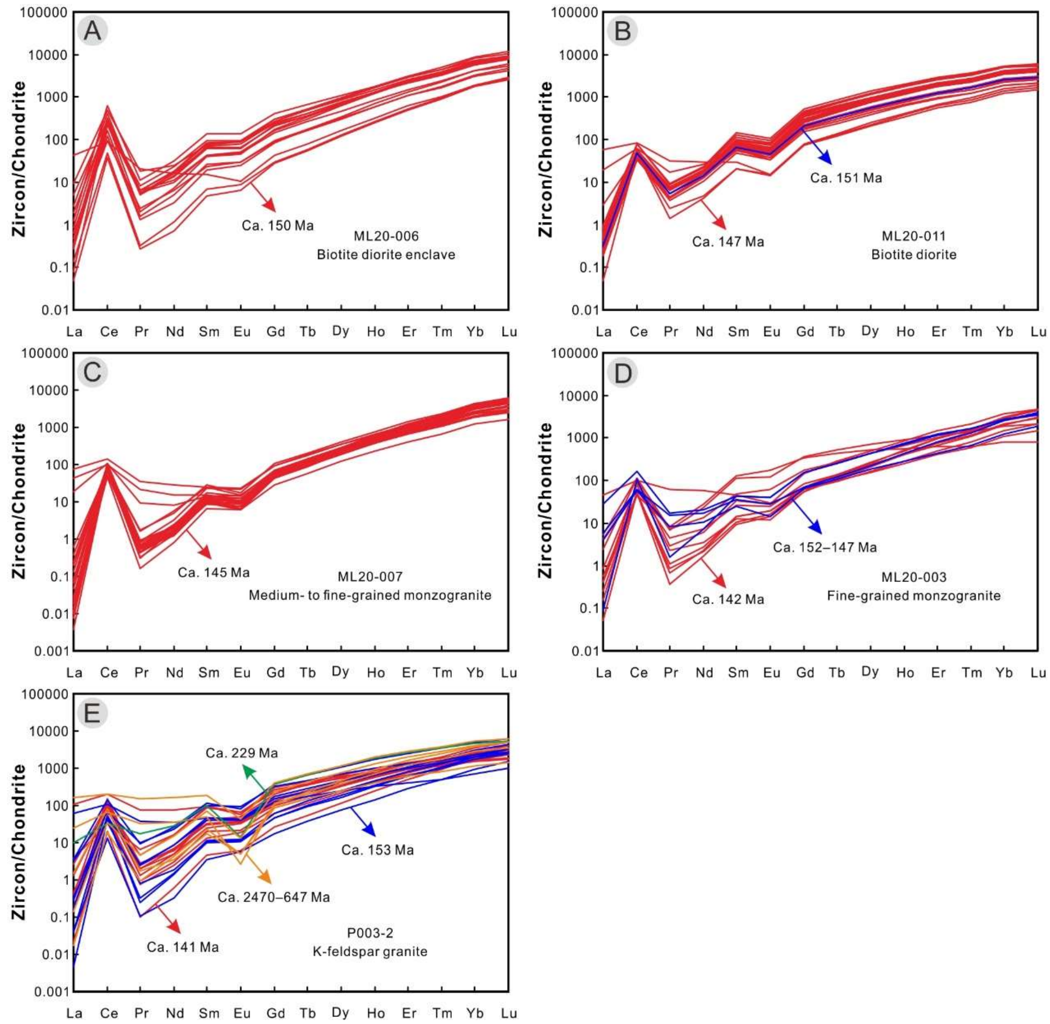

Figure S2. Chondrite-normalized rare earth element patterns of analyzed zircons for the Mangling intrusive complex. Normalizing values are from Sun and McDonough (1989).

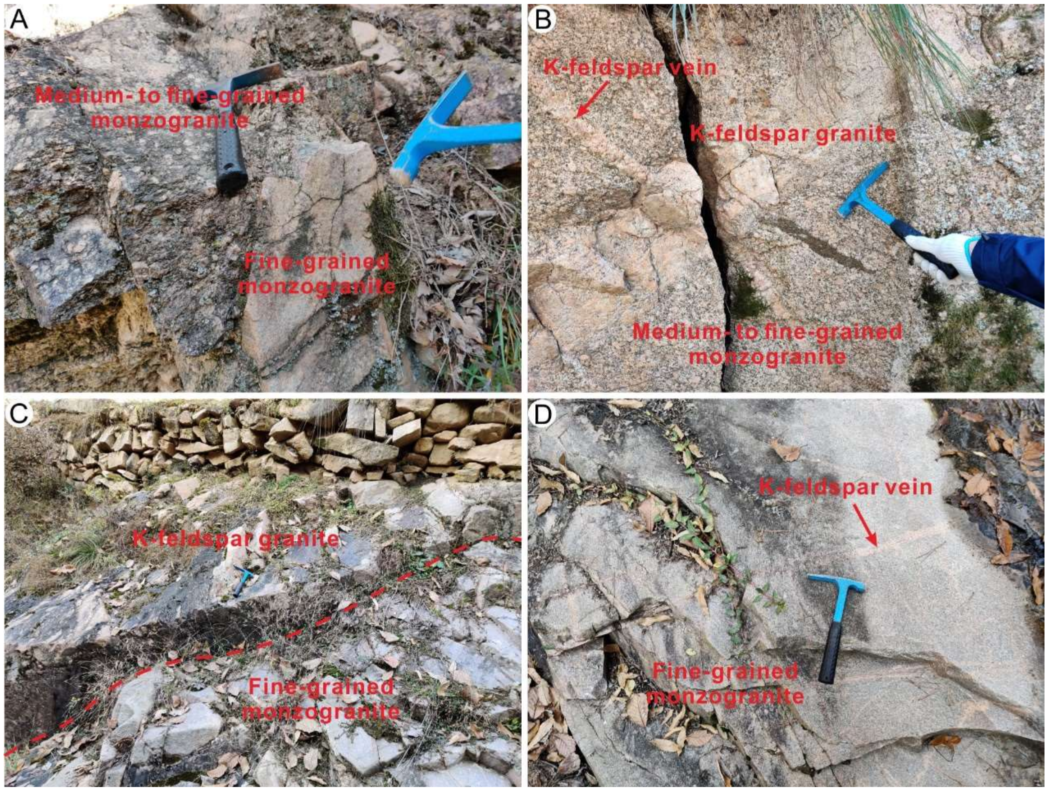

Figure S3. Field photographs showing relationships of the granitic rocks of the Mangling intrusive complex. (A) Medium- to fine-grained monzogranite was intruded by the fine-grained monzogranite. (B) Medium- to fine-grained monzogranite was crosscut by the K-feldspar granite and a K-feldspar vein. (C) K-feldspar granite intrudes into the fine-grained monzogranite. (D) Fine-grained monzogranite was crosscut by K-feldspar veins.

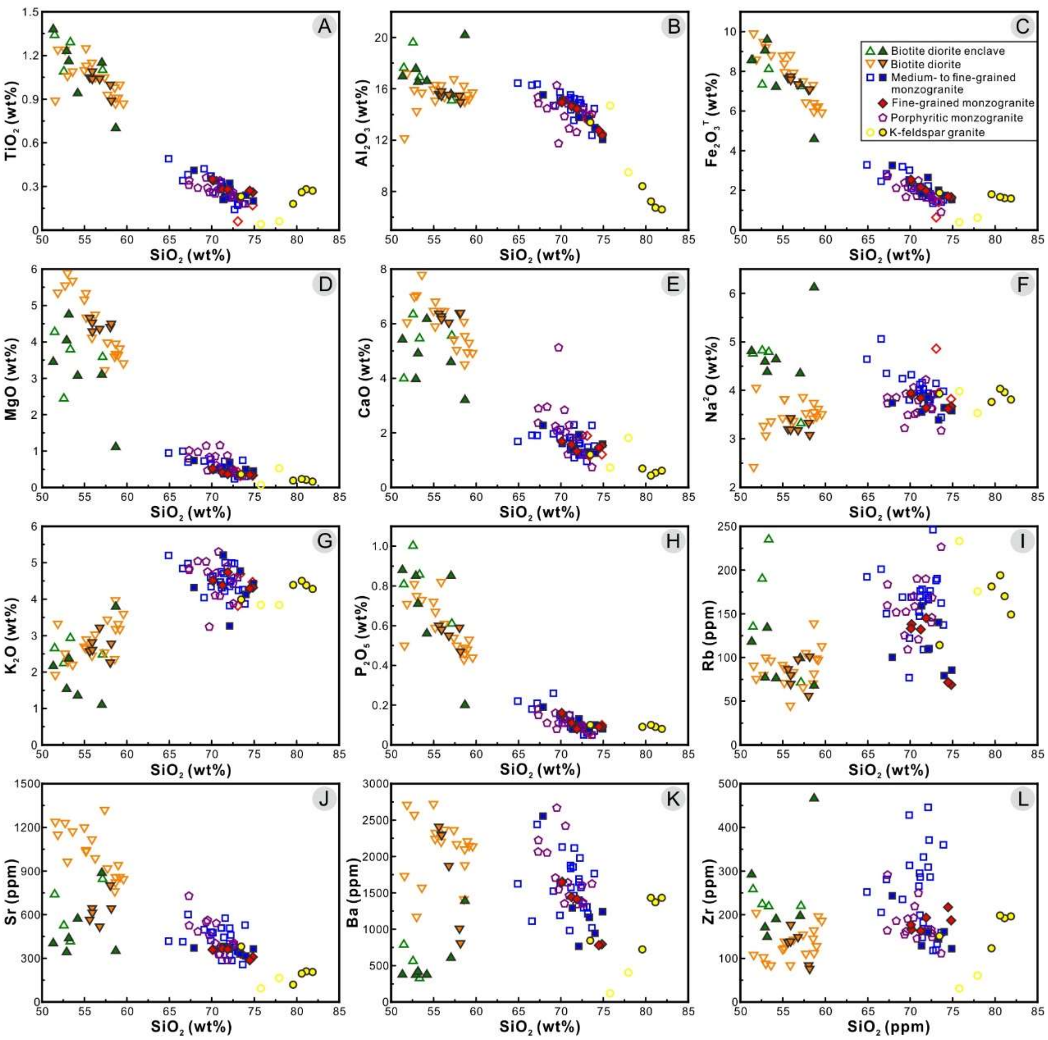

Figure S4. Harker diagrams of selected major and trace elements against SiO_2 for the Mangling intrusive complex. Published data of Mangling dioritic and granitic rocks are same as Fig. 5.

References

Sun, S.S., and McDonough, W.F., 1989, Chemical and isotopic systematics of oceanic basalts: implications for mantle composition and processes, In Saunders, A.D., Norry, M.J., eds., Magmatism in Ocean Basins: Geological Society, London, Special Publications 42, p. 313–345, https://doi.org/10.1144/GSL.SP.1989.042.01.19.